Tuning luminescence of 3d transition-metal doped quantum particles: Ni^{+2}: CdS and Fe^{+3}: CdS

S. M. Taheri* and M. H. Yousefi
Faculty of Sciences, Malek-Ashtar University of Technology, Isfahan, Shahin shahr, P.O. Box 83145/115, Islamic Republic of Iran

A. A. Khosravi
Departments of Physics, Shahed University, Tehran, Islamic Republic of Iran
(Received on 21 November, 2009)

The room-temperature photoluminescence of $Cd_{1-x}M_xS$ (M=Ni, Fe) nanoparticles were investigated. Compared with the photoluminescence of CdS which peaks at 475 nm, the photoemission of CdS:Fe nanoparticles was peaking at 537 nm because of Fe acting as luminescent centers. On the other hand, the green emission (503 nm) of CdS:Ni attributed to the $^1T_{2g}(D) \rightarrow {}^3A_{2g}(F)$ raditive transition. With the increase of the Ni^{+2} concentration, photoluminescence intensity is increased while by Fe replacement with Cd ions, PL intensity is decreased. Relative to bulk crystals, due to the quantum confinement effect the band gap of CdS clusters is significantly blue-shifted with decreasing cluster size. CdS nanoclusters present a mixed hexagonal/cubic structure and with increasing doping concentration the peaks position of doped CdS shifts to higher angle.

Keywords: Nanoparticles; Optical properties; Photoluminescence.

1. INTRODUCTION

Colloidal luminescent semiconductor nanocrystals (NCs), also known as quantum dots (Q-dots), have attracted considerable attention due to their significant potential application [1–3]. Quantum size effects (QSE) associated with the low dimensionality lead to several remarkable modifications in the physical properties of materials [4–6]. These effects are pronounced and lead to a discrete and size-dependent energy level structure when the cluster radius is typically less than the radius of bohr exciton [4, 7]. Cadmium sulfide is an $A^{II}B^{VI}$ compound semiconductor with a wide direct band gap of 2.42 eV (515 nm) and a small exciton Bohr radius of 2.5 nm. Owing to its wide band gap, it is used in violet and blue regions. A signifcant amount of current research is aimed at using the unique optical properties of Q-dots in devices, such as light-emitting diodes (LEDs), solar cells and biological markers [8]. 3d transition-metal impurities in semiconductors form deep levels within the band gaps of the host materials. They are technologically important as luminescence centers and charge compensations as well as unwanted traps. Since Bhargava et.al reported the novel properties in nanosized ZnS doped with Mn^{+2} ions [9], many studies have been published on Ti, V, Cr, Mn, Fe, Co, Ni, Cu and rare earth metal ions activated II-VI, III-V and I-III-VI nanometer scale semiconductor materials [10, 17]. Commonly used techniques for the synthesis of II-VI semiconductor Q-dots includes solid-state reaction, sol-gel, microwave electromagnetic radiation, hydrothermal [18–21]. During the wet chemical synthesis of nanoparticles, organic stabilizers are usually used to prevent them from aggregating by capping their surfaces. Here, we report the results of our study of the PL characterization of Ni^{+2} doped CdS Q-dots. Also the effects of major variable of the experimental condition, that is, the capping agent concentration, temperature and time on the physical properties of nanosized CdS particles.

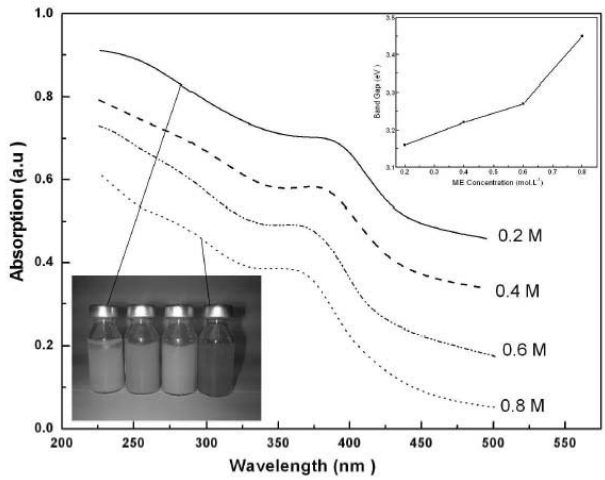

FIG. 1: Absorption spectra depict for the CdS Colloids Q-dots with different concentration of capping agent. Inset plot shows the relationship of band gap of Q-dots as a function of the ME concentration.

2. EXPERIMENTAL

Doped CdS nanoparticles were carried out by a chemical precipitation method which is very similar to described by Khosravi *et al.* [22]. Spherical particles with a very narrow size distribution can be obtained by controlling the synthesis parameters [22]. In a typical procedure, amounts of $CdCl_2.4H_2O$, $NiCl_2.4H_2O$ and $FeCl_3.3H_2O$ stock solutions and distilled water were added together to bring the concentration of Cd^{+2}, Ni^{+2} and Fe^{+3} of 0.01 mol.L^{-1}. For dopping with various amounts of Ni or Fe, (by volume) is added and stirred up to 2h. Mercaptoethanol (ME) was also added drop wise to the reaction medium which stabilizes the particle surfaces. The diluted $Na_2S.3H_2O$ solution of 0.1

*Electronic address: Sm.taheri59@gmail.com

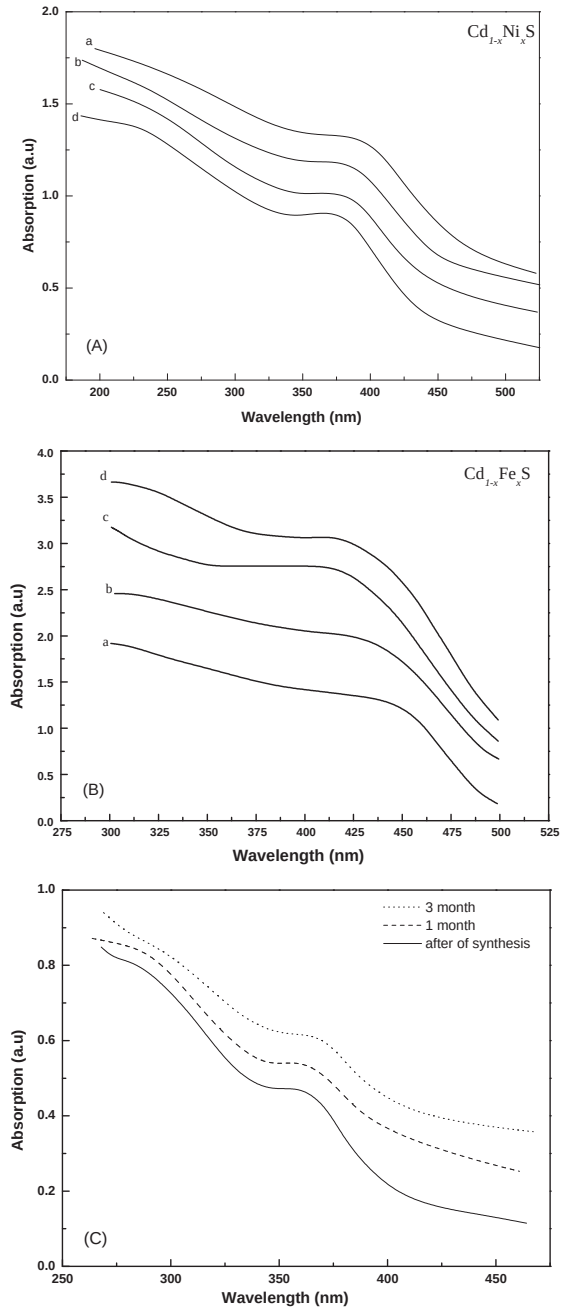

FIG. 2: UV-visible spectra of the CdS Q-dots doped with (a) Ni^{+2}; (b) Fe^{+3} under different concentrations of dopant [a: undoped, b:1%, c:3%, d:5%], and (c) absorption spectra are at different time.

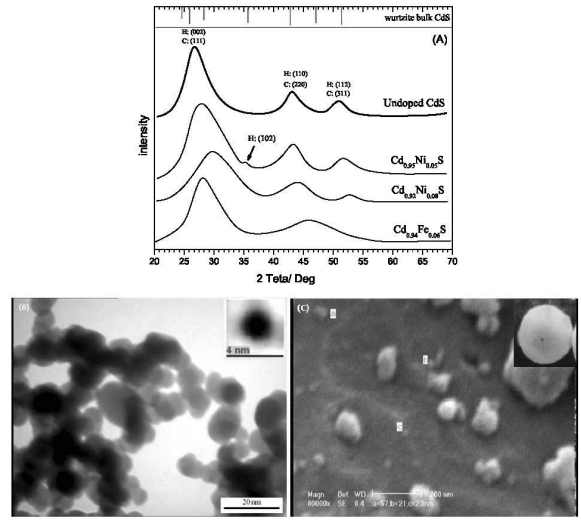

Fig. 3:(a)X-ray diffraction patterns, (b) TEM image and (c) SEM micrographs of doped CdS colloid Q-dots.

FIG. 3: (a)X-ray diffraction patterns, (b) TEM image and (c) SEM micrographs of doped CdS colloid Q-dots.

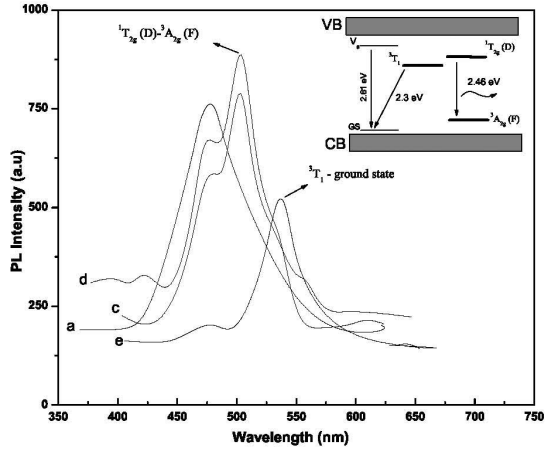

FIG. 4: PL spectra for CdS (a) and Cd $_{0.94}$ $Fe_{0.06}S$ (e) and $Cd_{1-x}Ni_xS$ colloids Q-dots with doping concentration x=0.01 (c), x=0.05 (d), respectively. Excitation wavelength is 344 nm. The inset energy band diagram shows the difference in radiative electronic transitions in doped CdS Q-dots.

mol.L^{-1} was added to this mixed Cd^{+2}, Ni^{+2}, and Fe^{+3} solution drop wise under vigorous stirring at room temperature with a small amount of surfactant. The colloidal samples washed in methanol to remove any excess sodium nitrate which may be present, and oven dried for 24 h at 40 °C. The experiments have been carried out under nitrogen atmosphere to prevent oxidation of clusters. The UV-Vis absorption spectra of 10 mM transparent solutions of nanoparticles were recorded by using an UV-Vis spectrophotometer Perkin-Elmer Lambda 2 at room temperature. Luminescence properties of the Q-dots were measured at room temperature by utilizing a LS-55 Spectrometer with excitation wavelength 344 nm in the spectral range 350-750nm. X-ray powder diffraction (XRD) patterns were recorded on a diffractometer D8ADVANCE model of BRUKER Company using Cu Kα irradiation (λ=1.5418 A°). The morphology of the colloids Q-dots were examined by a scanning electron microscopy (SEM, LEO-1455, Germany). The specimen was suspended in distilled water, dispersed ultrasonically to separate individual particles, and one or two drop of the suspension was deposited onto substrate and dried for 24 h at 40 °C. Transmission electron micrograph (TEM) of the nanoparticles were taken by a JEOL JEM-1200EXII electron microscope operating at 120kV. The supporting grids were

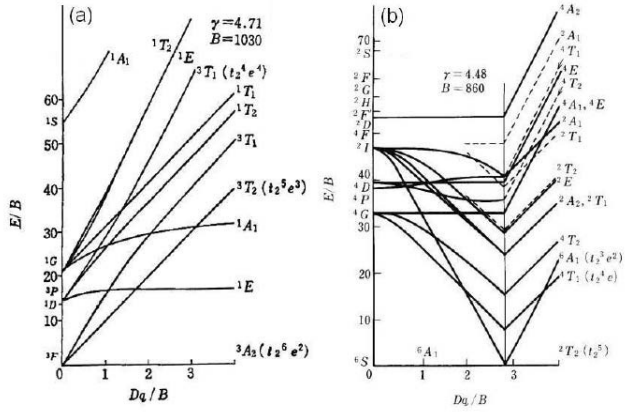

FIG. 5: Tanabe-Sugano diagrams for the (a) $^3d_8$ and (b) $^3d_5$ configuration coordination in crystal field [30].

formvar-covered, carbon-coated, 200-mesh copper grids.

3. RESULT AND DISCUSSION

To obtain semiconductor NCs the choice of the capping molecules is critical. If the bonding between capping molecules and NCs precursor is too weak, particle growth is fast and bigger crystallites are formed. If the binding is too strong, the NCs will not be formed. Fig. 1 shows absorption spectra of CdS Q-dots at different concentration of the capping agent. As shown in Table 1, with increase in the concentration of the ME from standard condition S_1 [$CdCl_2 \sim$ 0.01M, $Na_2S \sim$ 0.01M, ME $\sim$ 0.2M] to S_2 [$CdCl_2 \sim$ 0.01M, Na_2 S $\sim$ 0.01M, ME $\sim$ 0.8M], the particle size of the Q-dots increases from 3.51 to 3.02 nm. Here, the optical absorption coefficient decreases significantly with increase in the concentration of the ME from S_1 to S_2. The absorption edge shifts to lower values of wavelength for higher ME concentration S_2 and correspondingly, the E_g takes values from 3.29 to 3.62 eV respectively as shown in the inset plot of Fig. 1. A higher ME concentration also leads to more monodisperse particle size distribution.

System	x	C_2H_5OSH (M)	P_1/P_2	band gap (eV)	PS (nm)
CdS-S_1	-	0.2	-	3.29	3.51
CdS-S_2	-	0.8	-	3.62	3.02
a-Ni(Fe)$_x$	undoped	0.3 (0.01)	30$\sim$0.3/0.01	3.28 (2.83)	3.59 (5.17)
b-Ni(Fe)$_x$	0.01	0.3 (0.01)	30	3.32 (2.85)	3.51 (5.05)
c-Ni(Fe)$_x$	0.0.	0.3 (0.01)	30	3.36 (2.89)	3.43 (5.03)
d-Ni(Fe)$_x$	0.05	0.3 (0.01)	30	3.39 (2.93)	3.35 (4.63)

The optical absorption spectra of doped CdS Q-dots are shown in Fig. 2. The CdS colloids nanoparticles were prepared under standard conditions while for Ni^{+2} and Fe^{+3} dopant, the conditions were as follows: P_1 [$CdCl_2$- 0.3M, Na_2S- 0.3M , ME- 0.3M, $NiCl_2$- 0.3M] and P_2 [$CdCl_2$- 0.01M, Na_2S- 0.01M , ME- 0.01M, $FeCl_3$- 0.01M], respectively. It is clearly shown in Fig. 2 on increasing dopant concentration of dopant ions their absorption spectra shoulder is illustrated from 378(438) nm to 365(423) nm for $Cd_{1-x}M_xS$ (x=0-0.05) that shows a blue shift about 13(15) nm, respectively. Blue shifting in excitonic absorption peak (*i.e.* band gap increase; $E_g = hc/\lambda_{max}$) may attribute to the formation of smaller particles, which is due to the concentration of dopant% incorporated into the nanoparticles. A corresponding decrease in bandwidth is observed in the XRD pattern (Fig. 3a) of Ni^{+2} (Fe^{+3}) doped CdS nanoparticles. The apparent band gap of the CdS doped with Ni^{+2} and Fe^{+3} Q-dots is found to be significantly higher ($E_g \sim$ 3.39 and 2.93 eV, respectively) than that of CdS (2.42 eV). However reference [23] reported that the QSE in direct-gap semiconductor NCs were well understood, such as a shift of the optical absorption edge to higher energies with decreasing size, which can explain the UV-vis blue shift effect. Doped CdS particle size was also obtained from the band gap according to the effective mass approximation, which is summarized in Table1. The observed shift in band gap values with varying dopant% may be attributed to the change in energy eigen values as a result of perturbation potential due to exchange interaction. This observation is consistent with Gemma's suggestion that substitution of any transition metal impurity in CdS, ZnS, ZnO, and GaP changes the band gap values [24]. Fig. 2c shows that the absorption spectra of Ni^{+2} doped CdS nanoparticles obtained in different time, from which little change was observed for absorption onset, indicating that the size of CdS nanoparticles was not significantly influenced by time.

Fig. 3a shows the typical XRD (Cu-Kα radiation) pattern of the doped and undoped samples. The wide diffraction peaks suggested that the ultrafine particles were in poor crystallization. Here, difraction peaks associated with both cubic and hexagonal phases are obtained with a strong peak at 2θ=26.6° associated with the (002) reflection of wurtzite CdS or the (111) reflection of the zinc blend modification, which indicates a strong preferred orientation [25]. Besides this, two additional weak difraction peaks at 2θ=43.3° and 53° associated with the (110) and (112) reflection of the wurtzite modification or the (200) and (311) reflection of the zinc blend CdS structure are also observed. X-ray diffraction data reveals the diffraction peak of $Cd_{1-x}Ni_xS$ at (111) plane shifts to larger angle and lattice constant decreases with increasing Ni^{+2} concentration, which is due to replacement of Cd ions (0.96 A°) with smaller Ni ions (0.70 A°) in the host lattice. Also no characteristic peaks of impurity phases have been observed. From the Debye-Scherrer equation the average sizes of particles doped with different dopants, estimated from half width of these lines to be about 2.0-2.5 nm [26].

TEM image of the undoped CdS Q-dots is shown in Fig. 3b. The particles are most spherical and the average particle size is ca. 4 nm. But moderate agglomeration with a size as large as ca. 20 nm can be observed. The surface morphology of the CdS Q-dots (d$\sim$200 nm) prepared under standard conditions is seen in Fig. 3c (SEM). Here, formation of nanoclusters of size 20-60 nm is initiated, the grains group together to form domains in these NCs. The agglomeration of the particles observed in the SEM images was due to the drying process used in the preparation of the samples. Although particle agglomeration may be observed in the TEM images they do not coalesce together, maintaining their identity.

In the PL process, an electron from the CdS valance band is excited across the band gap and photo excited electron subsequently decay by a normal recombination process to some surface or defect states. The Fig. 4 shows the emission spectra of doped and undoped CdS Q-dots. The emission peak at 478 nm, related to the luminescence of CdS Q-dots, which is due to the radiative transition from the recombination of charge carriers of through the defect state. Defect states can be attributed to the presence of anion vacancies [27].

The ion Ni^{+2} (with ^3F ground state) has the electronic configuration $^3d_8$. Also the $^3d_5$ system iron (III) with sextet (^6S) ground state is well known activators in many minerals, (Fig. 5). When a metal ion occupies a certain position in a crystal, that affects the ion increases as the space containing the ion becomes smaller and with increase in crystal field strength, the energy for the above transition is predicted to decrease, hence emission shifts to longer wavelength [28]. Tanabe-Sugano diagrams demonstrate that those configurations in which the lowest excited levels (light-emitting levels) are located in the visible spectral region. For d_5 (see Fig. 5b), $^4T_1$ (^4G) is the lowest excited level, which is located in the visible region at weak crystal field of $D_q/B<1.5$. Mn^{+2} of this configuration, having the smallest D_q value among transition metal ions is a suitable activator for green-to red-emitting phosphors [28]. On the other hand, the lowest multiplet term ^3F of the free Ni^{+2} ion in split into $^1T_{2g}(^1D)$, $^3T_{2g}(^3F)$ and $^3A_{2g}(^3F)$ through the anisotropic hybridization [29,30]. Three luminescence bands in the near IR, red and green parts of the spectrum characterize Ni^{+2} in many synthetic luminofors [31]. For example, a broad IR band peaking at 1520 nm and connected with electron transition from the lowest excited state $^3T_{2g}$ has been found in enstatite artificially activated by Ni^{+2} [32]. Green luminescence is connected with $^1T_{2g}(D)\rightarrow {}^3A_{2g}(F)$ while the red one with $^1T_{2g}(D)\rightarrow {}^3T_{2g}(F)$ electron transition. About Fe ions, previous works show that entrance of Fe ions in a typical II-VI semiconductor such as ZnS, ZnSe, CdTe and CdS, due to crystal field effect leads to new energy states (i.e. $^3T_1$, $^5T_2$ and ^5E states) in the band gap of these materials [33-35]. Nevertheless, the green emission of $Cd_{1-x}Ni_xS$ (x=0.01 and 0.05) at 503 nm is due to the $^1T_{2g}(D)\rightarrow {}^3A_{2g}(F)$ transition of Ni^{+2} . On the other hand, the emission peaks at 537 nm for $Cd_{1-x}Fe_xS$ (x=0.06) Q-dots, can be attributed to the transition from the induced. The high luminescent intensity of $Cd_{1-x}Ni_xS$ (x=0.05) colloid Q-dots is due to the enhancement of radiative recombination in luminescent process ($^1T_{2g}(D)\rightarrow {}^3A_{2g}(F)$). The emission efficiency of Fe^{+3} doped CdS is lower than that of pure CdS, which can be attributed to the increase of nonradiation recombination. Since the ion radius of Ni^{+2}, Fe^{+3} and Cd^{+2} are 0.70 A°, 0.65 A° and 0.97 A°, respectively. Ni^{+2} and Fe^{+3} ions may be in Cd sites or as interstitial ions of CdS nanoparticles. When these ions are doped into the CdS nanoparticles, their deep enters are formed, which can inhibit more electrons (holes) to be excited and can lead to the enhancement of nonradiative recombination processes. As a result, their emission intensities become weaker than that of pure CdS nanoparticles [36].

4. CONCLUSIONS

In summary, solid solutions of $Cd_{1-x}M_xS$ (M=Ni^{+2}, Fe^{+3}) colloidal Q-dots with varied crystallite size 2-6 nm were successfully synthesized by a facile wet chemical technique. Due to the quantum confinement effect, the optical band gap increases compared with bulk materials, *i.e.* optical band gap of semiconductor NCs can be tuned as desired using the transition metal ions and capping agent in suitable concentrations. On the other hand, the absorption spectra show that the size of CdS: Ni^{+2} Q-dots was not significantly affected by the different time. XRD measurement confirms the structure, both cubic and hexagonal phases and peaks position of doped CdS shifts to higher angle with increasing dopant concentration. TEM and SEM studies indicated that doped CdS Q-dots are fairly uniform and spherical shape with approximate particle size 4-20 nm, respectively. The emission band of CdS Q-dots is at 475 nm which can be attributed to the transition of through defect states. Due to the $^1T_{2g}$ (D)$\rightarrow {}^3A_{2g}$ (F) transition of Ni^{+2} and $^3T_1$ levels of excited Fe ions to the ground state, the green luminescence bands at 503 nm and 537 nm occurs, respectively. The relative emission intensity of CdS Q-dots doped with Ni^{+2}(Fe^{3+}) is higher (lower) than that of pure CdS, which is due to the enhancement of radiative (nonradiative) recombination in luminescent process.

Acknowledgements

The authors would like to acknowledge Mr. O. Khani and M. Janesari from the NRG (Nanotechnology Research Group) for their contribution to this research project.

[1] X. Duan, Y. Huang, R. Agarwal, C.M. Lieber. Nature. **421**, 241 (2003)
[2] M.S. Fuhrer, J. Nygard, L. Shih, M. Forero, Y.G. Yoon, M.S.C. Mazzoni, H.J. Choi, Science.**288**, 494 (2000).
[3] Z.F. Ren, Z.P. Huang, J.W. Xu, J.H. Wang, P. Bush, M.P. Siegel, P.N. Provencio, Science.**282**, 1105 (1998).
[4] Y. Kayanuma, Phys. Rev. B **38**, 9797 (1988)
[5] P. Nandakumar, C. Vijatan, and Y. V. Murati, Opt. Commun.

Am. **185**, 457 (2000)
[6] S. M. Oak, K. S. Bindra, R. Chari, J. Opt. Soc. Am. B **10**, 613 (1993)
[7] Al. L Efors and A. L. Efors, Sov. Phys. Semicond. **16**, 772 (1982)
[8] K. S. Babu, T. R. Kumar, P. Haridoss, C. Vijayan. J. Talanta. **66**, 160 (2005)
[9] R. Bhargava, D. Gallagher, X. Hong, A. Nurmikko, Phys. Rev. Lett. **72**, 416 (1994)
[10] M. Jain, *II-IV Semiconductor Compounds*, World Scientifc Publishing Co. Pvt. Ltd., 1994, p. 105
[11] S.J. Xu, S.J. Chua, B. Liu, L.M. Gan, C.H. Chew, Appl. Phys. Lett.**73**, 478 (1998)
[12] R.N. Bhargava, D. Gallagher, T. Welker. J. Lumin. **61-62**, 275 (1994)
[13] Y. Wang, N. Herron. J. Phys. Chem. **95**, 525 (1991)
[14] W. Chen, F. Su, G. Li, A.G. Joly, Jan-Olov Malm, J. Appl. Phys. **92**, 1950 (2002)
[15] L.D. Sun, C.H. Liu, C.S. Liao, C.H. Yan, J. Mater. Chem. **9**, 1655 (1999)
[16] L.D. Sun, C.H. Liu, C.S. Liao, C.H. Yan, Solid State Commun. **111**, 483 (1999)
[17] L.D. Sun, B. Xu, X.F. Fu, M.W. Wang, Sci. China Ser. B **44**, 23 (2001)
[18] V. Stani, T.H. Etsell, A.C. Pierre, Mater. Lett. **31** , 35 (1997)
[19] T.A. Guiton, C.L. Czekai, C.G. Pantano, J. Non-Cryst. Solids. **121**, 7 (1990)
[20] H. Yang, C. Huang, X. Su, A. Tang, J. Alloys. Compounds. **402**, 274-277 (2005)
[21] T. Hanaoka, T. Taqo, M. Kishida, Bull. Chem. Soc. Jpn. **74**, 1349 (2001)
[22] A. A. Khosravi, M. Kundu, S. K. Deshpanda, Appl Phys Lett. **67**, 2702 (1995)
[23] Zhao XW, Komuro S, Aoyagi Y, Sugano T, Mat Sci Eng B-Solid. **51**, 154 (1998)
[24] N. Gemma, J. Phys. C: Solid State Phys.**17**, 2333 (1984)
[25] I. Kaur, D.K. Pandya, K.L. Chopra, Solid State Sci. Technol. **127**, 943 (1980)
[26] Kaeble EF, *Handbook of X-rays*, Mc Graw- Hill, NewYork, 1967
[27] A. Henglen, Top. Curr. Chem. **143**, 133 (3188)
[28] *Phosphor Handbook*, Phosphor research society, CRS Press.
[29] P. yang, M. Lu, D. Yuan, j. Shang, G. Zhou, Appl. Phys. A. **74**, 257-259 (3202)
[30] Kamimura, H., Sugano, S., and Tanabe, Y., *Ligand Field Theory and its Applications*, Syokabo, Tokyo, 3169 (in Japanese). With permission
[31] Blasse G, Grabmaier B (3194) *Luminescent materials*. Springer, Berlin Heidelberg New York
[32] MoncorgR, BettinelliM, Gyot Y, Girard S (3199) J Phys: Condens Matter 11:6831
[33] B. Tripathi, F. Singh, D.K. Avasthi, A.K. Bhati, J. Alloys. Com. **454**, 97 (3207)
[34] K. M. Donnell, K.M. Lee, G. D. Watkins. J. Phys. C solid state phys. **28**, 735 (3183)
[35] A. holda, A. Rodzik, A. A. Mielnikow, Phys. Stat. Sol. B **309**, 453 (3195)
[36] H. Yang, C. Huang, A. Tang, J. Alloy. Comp. **402**, 274 (2005)